Modeling intermolecular interactions of physisorbed organic molecules using pair potential calculations

Ingo Kröger, Benjamin Stadtmüller, Christian Wagner, Christian Weiss, Ruslan Temirov et al.

Citation: J. Chem. Phys. **135**, 234703 (2011); doi: 10.1063/1.3665923
View online: http://dx.doi.org/10.1063/1.3665923
View Table of Contents: http://jcp.aip.org/resource/1/JCPSA6/v135/i23
Published by the American Institute of Physics.

Modeling intermolecular interactions of physisorbed organic molecules using pair potential calculations

Ingo Kröger,[1,2,a)] Benjamin Stadtmüller,[1,2] Christian Wagner,[1,2] Christian Weiss,[1,2] Ruslan Temirov,[1,2] F. Stefan Tautz,[1,2] and Christian Kumpf[1,2,b)]
[1]*Peter Grünberg Institut (PGI-3), Forschungszentrum Jülich, 52425 Jülich, Germany*
[2]*Jülich-Aachen Research Alliance (JARA) – Fundamentals of Future Information Technology, 52425 Jülich, Germany*

(Received 28 June 2011; accepted 10 November 2011; published online 19 December 2011)

The understanding and control of epitaxial growth of organic thin films is of crucial importance in order to optimize the performance of future electronic devices. In particular, the start of the *submonolayer* growth plays an important role since it often determines the structure of the first layer and subsequently of the entire molecular film. We have investigated the structure formation of 3,4,9,10-perylene-tetracarboxylic dianhydride and copper-phthalocyanine molecules on Au(111) using pair-potential calculations based on van der Waals and electrostatic intermolecular interactions. The results are compared with the fundamental lateral structures known from experiment and an excellent agreement was found for these weakly interacting systems. Furthermore, the calculations are even suitable for chemisorptive adsorption as demonstrated for copper-phthalocyanine/Cu(111), if the influence of charge transfer between substrate and molecules is known and the corresponding charge redistribution in the molecules can be estimated. The calculations are of general applicability for molecular adsorbate systems which are dominated by electrostatic and van der Waals interaction.
 [doi:10.1063/1.3665923]

I. INTRODUCTION

The epitaxial growth of π-conjugated molecules on metal substrates is of highest interest in the field of organic electronics since the morphology of thin films plays a crucial role for charge transport.[1,2] Similar to inorganic semiconductors, a high crystalline quality, large grains and a low defect density can significantly improve the performance of organic-electronic devices such as organic light emitting diodes, organic field effect transistors, or organic solar cells.[3–6] Especially, a large overlap of the delocalized π-orbitals can improve the band transport in the direction of molecular stacking.

However, the morphology of the multilayer films strongly depends on the monolayer (ML) structure, since it acts as a template for further growth. Therefore, investigations of the submonolayer structures, epitaxy, and growth mode of these molecules on different (crystalline) substrates are of high interest. The superstructure formation in the first layer strongly depends on the adsorbate-substrate interaction and on intermolecular interactions. The latter usually are attractive due to van der Waals and Coulomb forces, but can also be repulsive as it was demonstrated for the family of metal-phthalocyanine molecules on Ag(111).[7–10] Fundamentally different growth modes of the planar adsorbed molecules are the consequence. This can even have consequences for the structural properties of thicker films and bulk-like material, which can be grown with very large crystalline grains or even as monocrystalline layers when the template effect of the first layer can be utilized.[7]

3,4,9,10-perylene-tetracarboxylic dianhydride (PTCDA, see Figure 1) is the most prominent example for an organic molecule which shows island-like growth when it adsorbs on weakly interacting surfaces such as Ag(111) or Au(111). An overall attractive intermolecular interaction leads to clustering of the molecules and to the formation of highly ordered islands having the "monolayer structure."[11,12] As long as the global coverage is smaller than one monolayer (1 ML), clean, uncovered regions exist between the islands which become smaller upon further deposition of molecules, while the islands grow in size. This growth behavior can directly be observed in photoelectron emission microscopy.[13] In low energy electron diffraction (LEED), it is indicated by diffraction images showing spots at fixed positions in reciprocal space which become more intense with increasing coverage. In most cases, this growth mode leads to a large number of different domains on the substrate terraces (and hence to a lot of domain boundaries) since the growth starts at many different nuclei at a time.

In contrast, the growth mode of copper-phthalocyanine (CuPc, see Fig. 1) on Ag(111) is dominated by intermolecular repulsion which causes a different scenario.[8] In the low coverage regime, the CuPc molecules behave like a two-dimensional gas (g-phase) whereby their nearest neighbor distance is maximized. In spot profile analysis LEED (SPA-LEED (Ref. 14)), this manifests itself in a diffuse ring structure having a radius that continuously rises with increasing coverage and indicates the reducing of the average

a)Present address: Physikalisch Technische Bundesanstalt, Bundesallee 100, 38116 Braunschweig, Germany.
b)Author to whom correspondence should be addressed. Electronic mail: c.kumpf@fz-juelich.de.

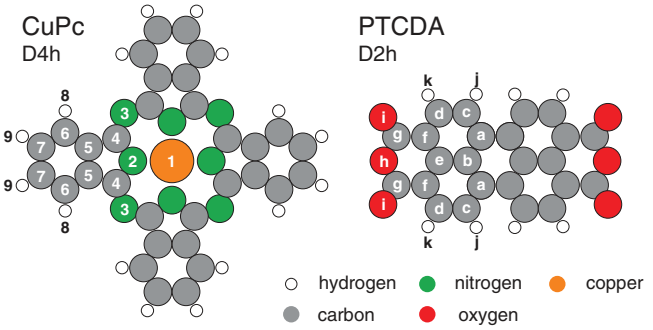

FIG. 1. Molecular structure of CuPc and PTCDA. The labels refer to the atomic partial charges in Table I.

intermolecular distance. Above a critical coverage of ≈0.9 ML, the molecular film becomes so dense that the molecules cannot move or rotate freely any more. The layer is then forced into a long range ordered superstructure with a point-on-line registry with the substrate (p.o.l.-phases).[15,16] When the coverage is further increased, this structure is continuously compressed, which can be seen from LEED patterns with continuously moving diffraction spots. The latter behavior proves the repulsive nature of the intermolecular interaction in the p.o.l.-phases of the CuPc molecules, which was also found for SnPc, TiOPc, and H_2Pc on Ag(111).[7,17–19] It was explained by donation of electronic charge from occupied molecular orbitals into the substrate and a consequent back-donation into unoccupied orbitals, which finally leads to a minimization of the total interface potential.[7,8]

This remarkable behavior – repulsive interaction between phthalocyanine molecules occurring in long-range ordered superstructures – appears to be limited to their adsorption on the Ag(111) surface. Investigations using a Au(111) substrate revealed that such an effect does not occur (or is very much weaker) due to the more weakly interacting surface and the missing charge transfer between molecules and surface.[9,10] Well-ordered structures found for CuPc/Au(111) at coverages above 0.93 ML give no indication for intermolecular repulsion. Only at lower coverages and RT, when intermolecular interactions are dominated by entropy effects, a similar behavior is found on both surfaces and disordered, gas-like phases occur. For details of the structural phase diagram, see discussions of Fig. 7 below, and Ref. 10. Regarding the submonolayer growth, we can conclude from these observations that CuPc – in contrast to PTCDA – grows as a diluted layer covering the surface homogeneously, even on weakly interacting surfaces where the molecules are very mobile. No island formation could be observed, indicating the absence of attractive intermolecular forces as they are found for most other molecules adsorbed on metallic surfaces. This raises the question under which conditions (molecular density, temperature, etc.) the interaction between these types of molecules is repulsive or attractive, and hence motivates the theoretical investigations presented in this work. We calculated the intermolecular pair potential for certain geometric arrangements using an ansatz comparable to the work of Wagner *et al.*[20] At first, we use the well-known model system PTCDA/Au(111) in order to benchmark our code and the utilized set of parameters. Then, the code is applied to explain the submonolayer growth of CuPc on Au(111). Finally, we give an outlook by testing a more strongly interacting surface, Cu(111), on which the CuPc molecules are rather strongly chemisorbed which leads to a fundamental alteration of the intermolecular interaction. Even for this system, the structure formation can be explained conclusively for both diluted and more compressed phases. This demonstrates the general applicability of our approach for organic adsorbate systems.

II. PAIR POTENTIAL CALCULATIONS

The pair potential Φ between two molecules A and B is defined as the total sum of the interaction potentials of every atom i of molecule A with every atom j of molecule B, whereby van der Waals ϕ_{ij}^{vdW} and electrostatic contributions ϕ_{ij}^{El} are considered. Both potentials are centrosymmetric and, hence, only depend on the distance r_{ij} between the atoms,

$$\Phi = \sum_i \sum_j \left(\phi_{ij}^{\mathrm{vdW}}(r_{ij}) + \phi_{ij}^{\mathrm{El}}(r_{ij})\right). \tag{1}$$

The following simplifications are made for calculating the individual contributions to the total potential.

(1) The electrostatic interaction potential is parameterized as a Coulomb potential between the atomic partial charges Z_i and Z_j,

$$\phi_{ij}^{\mathrm{El}} = \frac{Z_i Z_j}{4\pi\epsilon_0 r_{ij}}. \tag{2}$$

The molecules are treated as multipoles of point charges located at the atomic positions. The effect of image charges is neglected since the correct position of the image plane would be difficult to obtain, and fitting it would unnecessarily increase the number of free parameters. The results presented in the following justify this simplification.

A correct, quantitative treatment of the atomic charges within the molecules is difficult since density functional theory (DFT) calculations only yield the overall charge density of the molecule, and it is not *a priori* clear how to distribute the electron density between atoms. One possibility is the Mulliken population analysis[21] which in principle divides the "overlap population," i.e., the electron density mediating the bonding between the atoms, equally between two neighboring atoms. However, this procedure is strongly sensitive to the basis set used.

Therefore, we have chosen to use a natural bond orbitals (NBO) population analysis which better describes the atomic character.[22–24] In the NBO analysis, the atomic basis set from DFT is transformed into a basis of natural atomic orbitals (NAOs), which then have a fractional occupancy between 0 and 2. Adding all occupancies of the NAOs of each atom to the corresponding positive charge of the core leads to the partial charge of this atom within the molecule which can be used for the electrostatic potential calculations. The NBO charges of PTCDA and CuPc were calculated with the GAUSSIAN 03 package[27] (B3LYP functional, LANL2DZ basis set) and are

TABLE I. Atomic partial charges of PTCDA and CuPc derived from NBO population analysis.[27] The indices refer to atomic labels in Fig. 1.

CuPc				PTCDA			
1	+1.316	7	−0.204	a	−0.003	g	+0.817
2	−0.734	8	+0.235	b	−0.023	h	−0.578
3	−0.530	9	+0.223	c	−0.172	i	−0.539
4	+0.467			d	−0.127	j	+0.222
5	−0.074			e	−0.009	k	+0.254
6	−0.179			f	−0.146		

shown in Table I. The indices of the atoms correspond to the atomic labels in Fig. 1.

(2) The parameterizations of the van der Waals potential and the Pauli repulsion between two atoms i and j is given by

$$\phi_{ij}^{\mathrm{vdw}} = a_{ij}\exp(-b_{ij}r_{ij}) - c_{ij}/r_{ij}^{6}. \quad (3)$$

In literature, the parameters a_{ij}, b_{ij}, and c_{ij} are often called "non-bonding parameters" (in contrast to covalent "bonding" forces) and contain a Pauli repulsive part described by an exponential function, and an attractive London force proportional to r^{-6}. The latter can, in principle, be obtained from the atomic polarizability and an "effective" number of outer shell electrons by using the Slater-Kirkwood equation.[30,31] In Eq. (3), we choose a very universal approach for the non-bonding parameters because standard force field parameters (e.g., universal force field (UFF) (Ref. 14)) are in general obtained from fitting experimental data with a much larger set of parameters which also include bond stretching, bond angle distortions, electrostatic interaction, etc. These parameters are correlated to some extent, and hence, it might be erroneous to use only that subset of parameters which would be necessary for our approach.

All parameters, a_{ij}, b_{ij}, and c_{ij}, are element specific. For symmetric atomic pairs (i.e., when the atoms i and j are of the same type), they can be written as a_n, b_n, and c_n (with n = H, C, N, O, or Cu in our case). b_n and c_n can be found in literature[30,33,34] (see also Table II). The parameter a_n was chosen such that the position of the minimum of the resulting potential curve equals the non-bonding contact distances reported by Bondi *et al.*[35] For asymmetric atomic pairs, the parameters were approximated as the geometric mean of the corresponding parameters of symmetric pairs: $a_{ij} = \sqrt{a_n a_m}$ (n and m being the types of atoms i and j, respectively), b_{ij} and c_{ij} accordingly.[46] Table II summarizes the parameters used for

TABLE II. Coefficients of the van der Waals interaction and the Pauli repulsion as well as van der Waals radii used for the pair potential calculations according to Eq. (3). b_n are taken from Ref. 30, c_n mostly from Refs. 33 and 34, and r_{vdW} from Ref. 35.

n	a_n (eV)	b_n (Å^{-1})	c_n (eV Å^6)	r_{vdW} (Å)
H	432	4.52	1.96	1.30
C	34 000	4.59	15.70	1.77
N	9000	4.59	12.70	1.55
O	5600	4.59	9.41	1.50
Cu	550	2.95	94.93	1.40

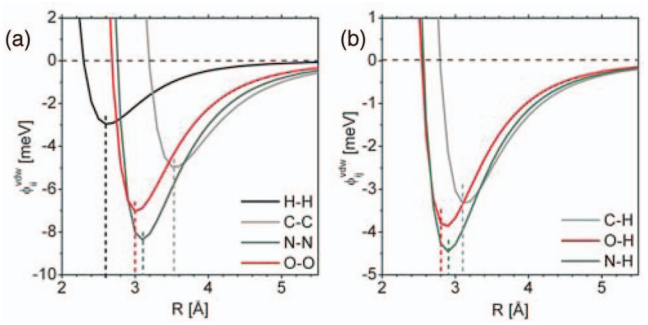

FIG. 2. Potential curves resulting from Eq. (3) for symmetric (a) and unsymmetric pairs (b). The vertical dotted lines indicate the corresponding sum of van der Waals radii.

the calculation, and Fig. 2 illustrates the resulting potential curves for symmetric and asymmetric pairs. The sum of the corresponding van der Waals radii is indicated by vertical dotted lines.

It should also be mentioned that – in extreme cases – other more sophisticated (and also more costly) methods of calculating the van der Waals parameters (e.g., *ab initio* methods) might result in slightly different potential curves. We have tested this for one specific system from literature, $CO_2\cdots CF_4$.[25] For these molecules, we calculated position and depth of the minimum in the potential energy using our pair-potential approach and found values which are very close to the numbers published in Ref. 25. This finding indicates that the basic parameter set we were using is well chosen. Furthermore, the comparison with experimental results discussed in the following and in Ref. 26 justifies our rather simple approach.

(3) The molecules are treated as rigid objects with a fixed inner geometry corresponding to the gas-phase geometry as it is derived from the state-of-the art DFT calculations (e.g., GAUSSIAN 03 (Ref. 27)). No molecular distortions upon adsorption on the surface or other effects are considered. This is justified by the experimental finding that the molecules under study (and also similar molecules) show no significant *lateral* distortions upon adsorption on metal surfaces. Only a bending was found rather frequently on more strongly interacting surfaces,[17,28,29] but this results in height differences of the atoms only and does not affect lateral distances significantly. Therefore, we can parameterize the distances r_{ij} between the atoms of two different molecules by the distance vector of the centers of the two molecules (ΔX, ΔY, ΔZ) and the orientation of the molecules relative to each other (Θ_X, Θ_Y, Θ_Z). (Θ_k stands for the rotation angle of molecule B relative to molecule A, around the k-axis.)

Based on these assumptions and the parametrization of the electrostatic and van der Waals interaction, the potential energy for any relative arrangement of two or more molecules can be obtained. We usually show two-dimensional maps of the energy potential which represent cuts or projections of a n-dimensional parameter space. In these maps, we typically vary the distance vector between the molecules in the xy-plane (parallel to the substrate surface, i.e., ΔX and ΔY) and the relative in-plane orientation of the molecules Θ_Z, while the vertical distance ΔZ and the rotation of the molecules

around the other axes (Θ_X and Θ_Y) are kept at fixed values. The energetic minima of such a map correspond to preferred relative positions of the molecules and should be reflected by the structures observed in the experiment.

In the following, such comparisons for three different systems are presented. The first, PTCDA/Au(111), is experimentally very well known and was used in order to verify the set of parameters which we have chosen, in particular the calculated partial charges. Further systems are CuPc/Au(111) and CuPc/Cu(111). Experimentally, all the systems have been investigated using SPA-LEED, x-ray standing wave (XSW), and scanning tunneling hydrogen microscopy (STHM),[8–10,36–39] a combination which allows very accurate measurements of the lattice parameters and the location and orientation of the molecules within the unit cell. STHM shows the geometry of the adsorbates rather than their electronic structure, and is therefore particularly suited for this investigation.

III. PTCDA/AU(111)

PTCDA/Au(111) is known for only weak adsorbate-substrate interactions having no dominant effect on the superstructure formation.[40] Therefore, we can expect that our pair-potential calculations give realistic results, although they do not take any substrate effect into account. The weakness of the interaction is, e.g., indicated by the molecular superlattice which is only of point-on-line coincidence with the underlying substrate.

The submonolayer growth of PTCDA/Au(111) is dominated by intermolecular attraction which is responsible for the formation of long range ordered islands. Two molecules per unit cell arrange themselves in a herringbone structure which is very similar to the (102) plane of the bulk structure.[11] Figure 3 shows an STHM image of an island of PTCDA/Au(111). The unit cell derived from this image (see green vectors in the figure) has the dimensions $|\vec{a}| = 19.2$ Å, $|\vec{b}| = 12.3$ Å, and $\gamma = 90°$. Identical numbers were found in earlier SPA-LEED investigations by Kilian *et al.* for the so-called "structure A."[12]

From this image, the lateral adsorption geometry can be extracted with rather high precision: Each PTCDA molecule has six neighbors. Two of them are translationally equivalent to the original molecule (equivalent molecules in the neighboring unit cells) and, therefore, have the same azimuthal orientation. Their distance vectors to the original molecule (red arrows in Fig. 3) are identical to the unit cell vector $\vec{b}$ ($|\vec{b}| = 12.3$ Å). The angle between the long molecular axis M1 of these molecules and vector $\vec{b}$ is 39°. The other four neighbors have an azimuthal alignment which differs from the original molecule by ($\angle_{M1,M2} = 101°$). Their distance vectors are $\pm\vec{c}$ and $\pm\vec{d}$ (blue arrows in Fig. 3), equal in length, but a little shorter than $\vec{b}$: $|\vec{c}| = |\vec{d}| = 11.4$ Å. The angles between the molecular axis M1 and the vectors $\vec{c}$ and $\vec{d}$ are 84° and 18°, respectively.

We now use these experimental findings to test our pair potential calculations. Under the only assumption of planar adsorption on the surface, we calculated the pair potential energies for all possible arrangements of two molecules. This

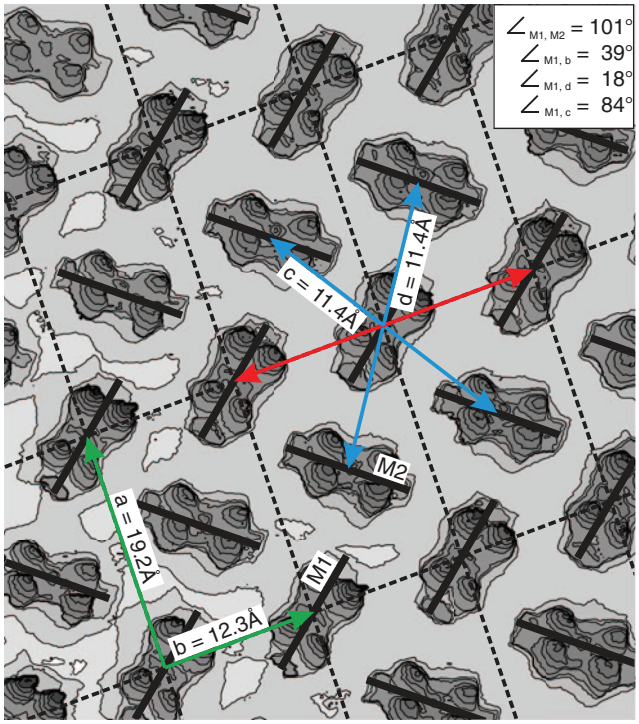

FIG. 3. Scanning tunneling hydrogen microscopy image of the PTCDA/Au(111) herringbone structure. The lattice spanned by the unit cell vectors $\vec{a}$ and $\vec{b}$ is indicated by the dotted lines. The two molecules (M1, M2) within the unit cell are rotated by 101° with respect to each other. The six neighbors of one PTCDA molecule are indicated by red and blue arrows.

means that the lateral distance vector (ΔX, ΔY), as well as the relative rotation of the molecules Θ_Z, was varied independently, whereby the vertical displacement ΔZ and the rotations around in-plane axes Θ_X and Θ_Y were fixed at zero. The long molecular axis M1 was arbitrarily set parallel to the ΔX axis. Figs. 4(a)–4(d) show the results, the pair potential energy Φ as a function of ΔX and ΔY, for a selected number of different rotation angles Θ_Z between 0 and 90°. Parts (a) and (e) of the figure are for the orientations found in the experiment: $\Theta_Z = 0°$ and $\Theta_Z = 101°$.

These maps can be understood as follows: Each point in the map corresponds to a distance vector (ΔX, ΔY) between the centers of the two molecules. For short vectors ending within the white area in the center of the map, the distance is so small that the molecules would be overlapping (or some atoms would have an unrealistical short distance of less than 1.0 Å). Therefore, the calculation is not performed within this area. The adjoining black-coded area indicates a region in which the repulsive part of the pair potential is still highly dominant (large positive values for the pair potential: $\Phi > 5.0$ eV). Outside of this area, the color code gives the calculated pair potential energy corresponding to the relative molecular geometry given by the parameters (ΔX, ΔY). All other parameters [ΔZ and (Θ_X, Θ_Y, Θ_Z)] are kept constant.

All energy maps contain both repulsive and attractive areas, depending on the relative position of the molecules and whether the electrostatic term is dominated by O–O and H–H interaction (repulsive) or O–H interaction (attractive). For example, in map (a) showing the case of identically

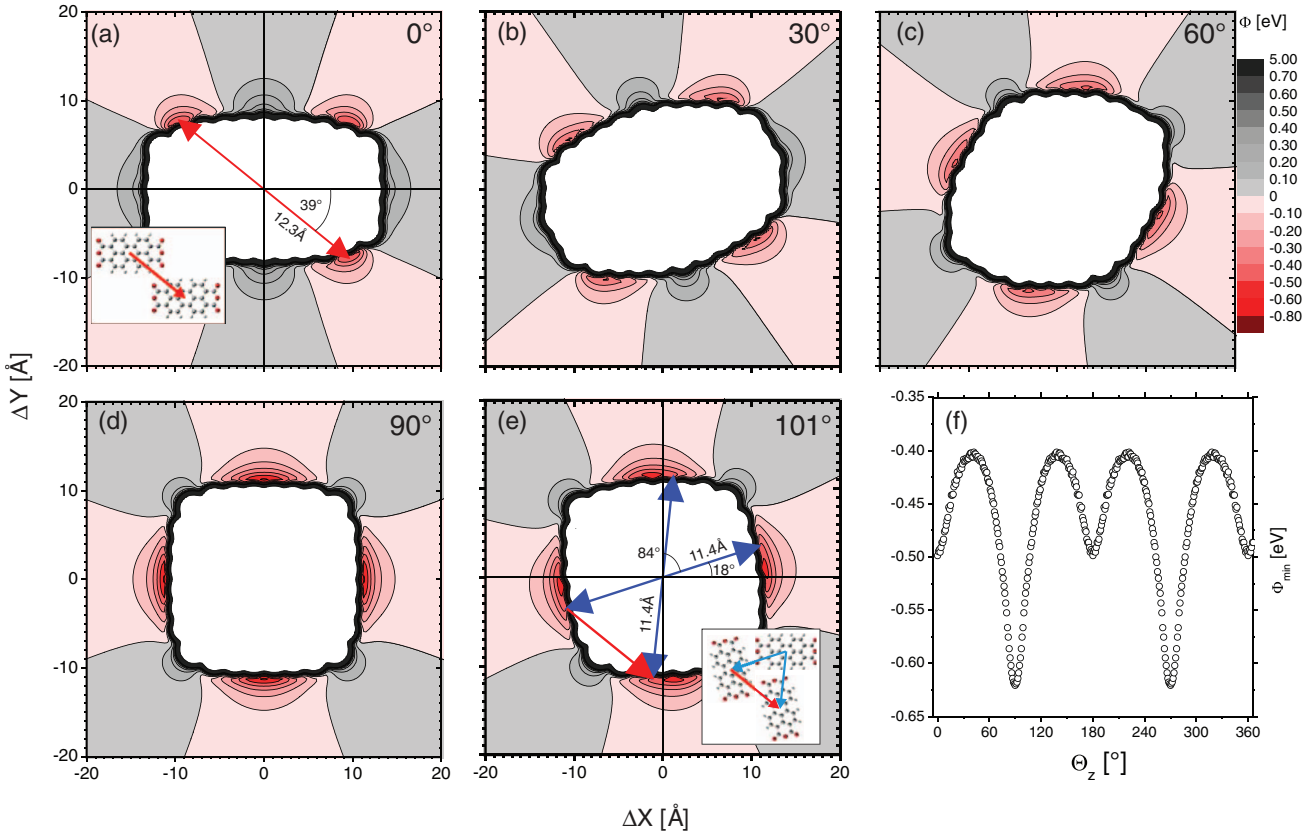

FIG. 4. (a)–(e) Pair potential maps for five different rotational orientations of two PTCDA molecules between $\Theta_Z = 0^\circ$ and $\Theta_Z = 101^\circ$. ΔZ, Θ_X, and Θ_Y are zero in all cases. Gray areas indicate repulsion between the molecules, red areas indicate attraction. Red and blue arrows in (a) and (e) denote the distance vectors between neighboring molecules as they were determined experimentally from the STHM image (Fig. 3). The insets in (a) and (e) illustrate the corresponding geometries. Panel (f) shows the minimum value of Φ extracted from the (ΔX, ΔY)-maps for each rotation angle Θ_Z, plotted versus Θ_Z. For details see text.

oriented neighbors, it can be seen that along the lines with either $\Delta Y = 0$ or $\Delta X = 0$ (i.e., for a linear arrangement of the molecules along their symmetry axis) only repulsive configurations occur, independent of the distance. This allows the conclusion that a brick-wall structure is energetically not favorable and explains that this structure was not observed in the experiment. Map (a) also shows four distinct and rather sharp minima at (ΔX, ΔY) = (± 9.5 Å, ±7.5 Å), which are −0.53 eV deep. They very accurately coincide with experimentally obtained distance vectors between identically oriented molecules which are shown in the figure as red arrows. The corresponding molecular arrangement is shown in the inset. This distance vector is identical to the unit cell vector $\vec{b}$ observed in the experiment.

We have calculated pair potential energy maps for all possible orientation angles Θ_Z between 0° and 360° in steps of 1° and show five of them in Fig. 4. Due to the symmetry of the molecule, each of these maps contains four symmetrically equivalent minima, the depths of which depend on the rotation angle. In Fig. 4(f), the Φ-value of these minima, extracted from each of the (ΔX, ΔY)-maps, is plotted versus the corresponding rotation angle Θ_Z. Thus, this panel shows how the depth of the minima from the (ΔX, ΔY)-maps change with changing orientation angle. The minima in this plot – two types of minima are found, one at 0° and 180°, the other at 90° and 270° – correspond to the ideal geometries of two flat-lying molecules on a non-interacting surface.

As already discussed above, the geometry corresponding to one of the minima (that one at $\Theta_Z = 0^\circ$) is also found in the experiment (see Fig. 4(a)). The other, significantly deeper minimum in Fig. 4(f) at $\Theta_Z = 90^\circ$ – the (ΔX, ΔY)-map is shown in Fig. 4(d) – is not found in the experiment. Instead, the second observed configuration corresponds to an angle of $\Theta_Z = 101^\circ$, the potential map is plotted in Fig. 4(e). The four minima in this map are significantly broader in azimuthal than in radial direction. The precise geometries found in the experiment (blue arrows) clearly lie in the region of negative potential (i.e., they indicate intermolecular attraction, corresponding energies are $\Phi_{18^\circ} = -0.42$ eV and $\Phi_{84^\circ} = -0.44$ eV), but they do not coincide with the minimum of $\Phi_{\min} = -0.58$ eV. The reason is that this calculation only considers pairs of molecules, i.e., the interaction between *two* molecules. However, when we take a third molecule into account, as it is indicated by the inset of Fig. 4(e), two of them are identically oriented and, hence, take up a relative position to each other according to the minimum in map (a), corresponding to the red distance vector. Since this minimum is very sharp, no big variation can be expected for length and direction of their distance vector (the red arrow). In other words, taking into account the third molecule means connecting the heads of the

two blue arrows in Fig. 4(e) by the relatively stiff red arrow. The figure illustrates that this is not possible without deflecting the blue arrows away from the minima in the map to those positions which are drawn in the figure. Hence, the arrangement of three molecules compromises slightly between the ideal relative positions of the three pairs of molecules, mostly at the expense of the blue arrows since they lie in rather shallow minima.

This explanation for the difference in the experimental and theoretical value for the optimum rotation angle ($\Theta_Z = 101^\circ$ and 90°, respectively) is somewhat qualitative. In a second step, we, therefore, tried to simulate a more realistic scenario and calculated the precise position and orientation of a molecule relative to all of its six nearest neighbors. The only constraint used is the unit cell size as found in STHM and LEED, and the fact that there are two inequivalent molecules in the unit cell. One molecule was put in the corners of the unit cell, the other must then roughly be positioned in the middle of the cell, but its precise position was varied in the following. Other parameters were the rotations of both molecules relative to the unit cell. This results in the arrangement shown in Fig. 5 with four independent parameters: the lateral position (X, Y) of the second molecule (identical to the distance vector between both molecules (ΔX, ΔY)), and the azimuthal orientation angles for both molecules. Figs. 5(a) and 5(b) show cuts through this four-dimensional parameter space. In Fig. 5(a), the energy potential is plotted versus (ΔX, ΔY) for fixed rotation angles (those giving the best energy potential) and yielded a molecule precisely centered in the cell as the best position. Due to steric conditions, the region for possible positions for the second molecule is small and lies close to the center of the unit cell. Map (b) is plotted versus both rotation angles for the second molecule being centered in the cell. Also here the result is unambiguous: Only in a small range of orientations, the molecules do not overlap, and only one clear and deep minimum is found in this range. It is located at $\Theta_{Z,1} = 40^\circ$ and $\Theta_{Z,2} = 140^\circ$, very close to the experimentally observed angles of 39° and 140° reported above. It should be mentioned again that the only constraint for this simulation was the unit cell size, and that the interaction to all six nearest neighbors were taken into account.

Furthermore, we have tested our code by simulating the vertical stacking of PTCDA molecules in three-dimensional islands. Experimentally, two different phases were found for the multilayer growth of PTCDA (the so called α- and β-phase). In both, the molecular layers have the same stacking distance of 3.2 Å.[33,41] The bulk geometry is shown as inset in the lower right of Fig. 6. We varied the parameters ΔX, ΔY (lateral shifts), and ΔZ (stacking distance) independently for two PTCDA molecules orientated parallel to each other. In Fig. 6, a two-dimensional cut through this three-dimensional parameter space is shown, which contains the absolute minimum of the calculation at (ΔX, ΔY, ΔZ) = (2.8, 0.0, 3.2) Å. Broad minima can be seen which are smeared out in ΔX-direction, but relatively sharp in ΔZ-direction. The right part of the figure shows a cut through the minimum in the pair potential map at $\Delta X = 2.8$ Å in ΔZ-direction and reveals the sharpness of the minimum. With 3.2 Å, it perfectly matches the π-stacking distance found in the experiment. The same

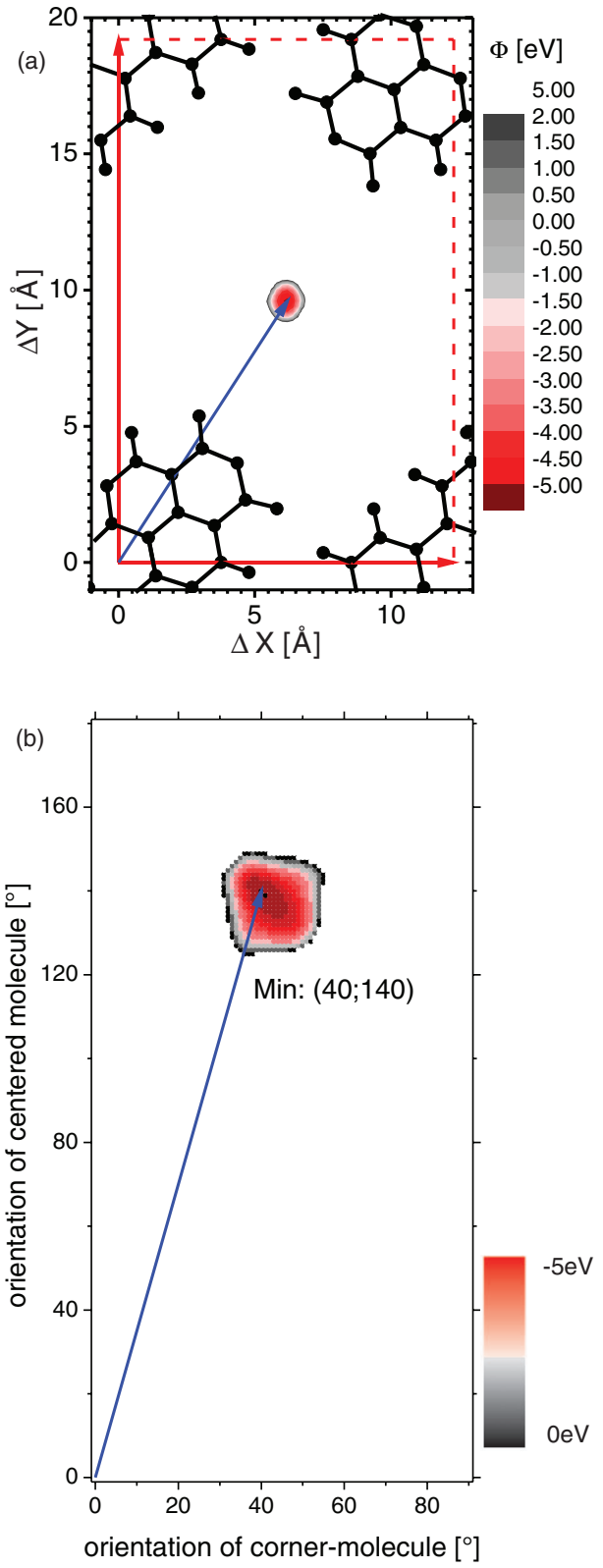

FIG. 5. Pair potential maps for the interaction of one molecule with its six nearest neighbors in the unit cell for PTCDA/Au(111). In (a), the result for the variation of the distance vector is shown. The allowed range lies only between 5.5 Å and 7.0 Å for ΔX and 8.5 Å and 10.5 Å for ΔY. The minimum is located precisely in the center of the unit cell. The central molecule and two of its symmetrically equivalent neighbors (at the left and right) are not drawn since their position is varied in this plot. In (b), the azimuthal orientations of both molecules were varied. Angles are measured between the long molecular axis and the long vector of the unit cell. The minimum is found for angles of 40° and 140° for the corner- and center-molecule, respectively.

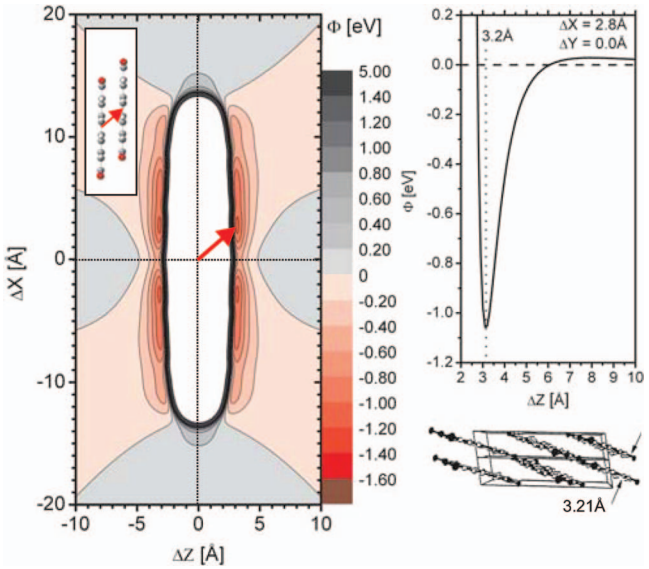

FIG. 6. ΔX-ΔZ pair potential map for PTCDA molecules arranged in π-stacking direction ($\Delta Y = 0$). In the right, a cut in ΔZ direction through the minimum at $\Delta X = 2.8$ Å and $\Delta Y = 0$ is shown. The minimum corresponds nicely to the molecular stacking geometry of a bulk crystal shown in the inset.

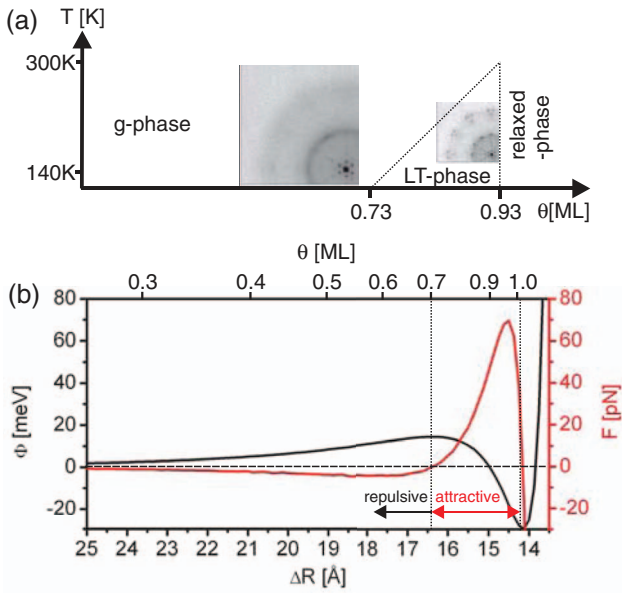

FIG. 7. (a) Structural phase diagram of CuPc/Au(111), taken from Ref. 10. (b) Calculated pair potential (black) and its gradient (red) plotted versus the radial displacement along the $\vec{b}$ direction (distance of the two molecules) and versus coverage (nonlinear scale at the top).

result was obtained for calculations considering two parallel layers of molecules, which both consist of molecules in the herringbone-arrangement known from the PTCDA α-phase.

The results of our calculations explain the experimental findings for both the lateral arrangement of PTCDA in monolayers on a non-interacting surface, and the vertical stacking in three-dimensional islands and bulk crystals. This indicates that a useful parameter set for the force field calculations was found. We can not only reproduce geometries found experimentally, but also predict the structure formation of similar systems (at least) qualitatively by using a minimum of constraints.

IV. CUPC/AU(111)

The lateral structure formation of CuPc/Au(111) is experimentally well investigated. It differs fundamentally from the situation for PTCDA/Au(111) due to the absence of island formation. In this section, we explain this behavior with our pair potential calculations, but at first briefly summarize the experimental data.

The physisorptive bonding character of the CuPc molecules to the Au(111) surface is proven by photoemission experiments[10] which indicate no significant charge transfer. This is in agreement with a measurement of the adsorption height by x-ray standing waves[9] that resulted in a value of ≈3.3 Å. Hence, also for this system, the substrate has only minor impact on the lateral structure formation.

The structural phase diagram (see Fig. 7(a) and Ref. 10) with its large region of disordered gas-like phases, the LT-phase transition, and the relaxed p.o.l.-phase at higher coverage, was already discussed in the Introduction. The basic details of the lateral structures – unit cell parameters of the LT-phase relative to the reconstructed Au(111) surface, intermolecular distances d in the g-phase and their dependence on coverage, as well as the critical coverage of the phase transition – are known from the SPA-LEED experiments.[10] Now, we want to address the fundamental question whether the general behavior of this system can be understood from our pair potential calculations alone.

At first, we concentrate on the ordered phases. Since all ordered structures of CuPc/Au(111) have only one molecule per unit cell, an equal orientation of the molecules can be assumed. The corresponding pair potential map for a lateral arrangement of two equally oriented CuPc molecules is shown in Fig. 8. Just like in the case of PTCDA discussed above, the only constraint we use for the calculations is the unit cell (in this case even only the information that there is just one molecule in the unit cell). Note that the energy scale in the map shown in Fig. 8 is smaller by one order of magnitude compared to those for PTCDA, which demonstrates a much weaker lateral intermolecular interaction of CuPc. In fact, the corrugation of the potential is only of the order of k_BT. This explains the experimental finding that – in contrast to PTCDA – no well-ordered structure or island formation is observed at RT. The intermolecular interaction is too weak to force the molecules into a long-range ordered pattern.

However, some local minima can be seen in the potential map (indicated in red, closeup in Fig. 8(b), which have a depth of $\Phi \approx -30$ meV. Hence, at low temperature, molecules can be trapped in these minima leading to a long-range ordered structure. This corresponds to the low temperature phase transition from the disordered g-phase to the LT-phase which was experimentally observed at coverages between 0.73 ML $\leq\theta \leq$ 0.93 ML (see structural phase diagram shown in Fig. 7(a)).

The unit cell of the LT phase is well known. Its parameters are $|\vec{a}| = 14.00$ Å, $|\vec{b}| = 14.1$ Å, and $\angle_{\vec{a},\vec{b}} = 91.7°$.[10] As can be seen in Fig. 8, a configuration can be found in which the unit cell vectors lie in close vicinity to the potential

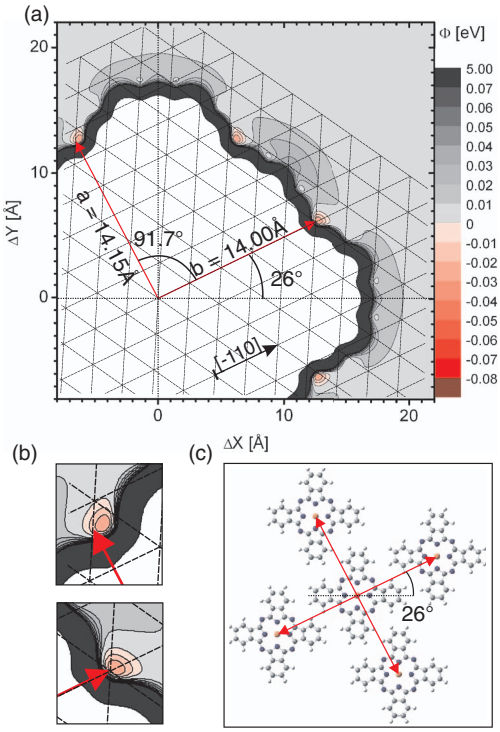

FIG. 8. (a) Pair potential map of equally oriented CuPc molecules. The lattice vectors of the LT-phase structure ($\vec{a} = 14.15$ Å, $\vec{b} = 14.00$ Å) lie close to the minima of the potential map, if the superimposed experimental unit cell and lattice of the reconstructed Au(111) surface are rotated by 26° relative to the molecular axis. (b) Vicinity of the minima of the potential map. (c) Corresponding real space model.

minima. The orientation of the molecules is then given by an angle of $\angle_{M1,\vec{a}} = 26°$ between the molecular axis M1 and the unit cell vector $\vec{a}$. This geometry is also illustrated in the real space model of Fig. 8(c). Note that the superstructure would be incommensurate if the unit cell vectors matched the potential minima precisely. Apparently this is not the case. The reason might be a small energy gain caused by a point on line registry with the substrate lattice which is enabled by the small deflection of the unit cell vectors from the ideal positions.

A second experimental observation is that the LT-phase is formed only in a rather small coverage regime and – in particular – not at coverages below 0.73 ML. This can be understood by a closer look at the radial shape of the potential variation along the LT-phase unit cell vector $\vec{b}$ through the potential minimum, as it is shown in Fig. 7(b): A potential barrier is found with a maximum at $\Delta R = 16.4$ Å which separates the global minimum at $\Delta R = 14.2$ Å and the sloping region for $\Delta R > 16.4$ Å. The red curve represents the derivative of the pair potential curve and, hence, corresponds to the force F between the two molecules. It shows that for an intermolecular distance of $\Delta R \geq 16.4$ Å, the intermolecular interaction is repulsive, while for 14.1 Å $\leq \Delta R \leq 16.4$ Å it is attractive. In an earlier work,[10] we have evaluated the g-phase quantitatively using SPA-LEED and found $\theta = [11.36 \text{ Å}/(\Delta R - 2.92 \text{ Å})]^2$ as the relation between the intermolecular distance ΔR and the global coverage θ. This relation is inverse parabolic; the offset term stems from the size of the molecules. Applying this equation to the abscissa of Fig. 7(b) results in the nonlinear scale given at the top of the figure and allows a direct comparison with the phase diagram (part (a) of the figure). It reveals that the minimum coverage, for which the LT phase transition was observed (0.73 ML), corresponds very well to the maximum in the pair potential and the crossover-point between repulsive and attractive intermolecular forces.

This finding is the key for understanding the phase formation of g-phase and LT-phase, as well as the progression of the corresponding phase boundary. For low coverages (<0.7 ML) the molecules have an average distance corresponding to the repulsive interaction regime shown in Fig. 8(a). However, their thermal energy kT and the height of the potential barrier between the repulsive and the attractive regime are in the same magnitude, and hence, the molecules enter (and also leave) the attractive regime with a certain rate. Although the barrier height for leaving the attractive regime is higher than for entering it, most molecules will be able to leave the attractive regime again so that no ordered structure will be formed at low coverage (g-phase regime). (Note that for most relative positions of the molecules, their interaction is *always* repulsive (see Fig. 8(a)). Only for few specific relative positions, attractive minima occur in the pair potential map. Since the molecules can still freely rotate and move at small coverages, only very few molecules have the chance to form clusters.)

Upon increasing the coverage, the rates for passing the barrier are changing. Due to a reduced average intermolecular distance, the attempt frequencies change, in particular for the direction towards the attractive regime. When the critical coverage (0.7 ML at LT) is reached, i.e., when the average distance drops below $\Delta R = 16.4$ Å, most molecules find themselves within the attractive potential regime. Although it is energetically possible to leave that regime, those molecules will quickly be trapped by a third, neighboring molecule, or reflected and re-trapped by the first partner molecule. Consequently, the molecules can now be trapped effectively in the attractive regime of the interaction potential, which leads to the formation of ordered islands on the surface.

The experiment reveals that the critical coverage for the formation of ordered structures is temperature dependent. At lower temperature, a smaller coverage is sufficient to force the molecules in ordered structures. Obviously, upon cooling, the molecules are increasingly hindered in leaving the attractive regime, i.e., the transmission rate for that process is more strongly reduced than for the direction into the potential minimum. This can qualitatively be understood by the height difference of the potential barrier, ≈50 meV for leaving and ≈20 meV for entering the attractive regime.

However, the temperature effect appears to be secondary. The coverage plays the dominant role in this behavior. Above 0.93 Å, the molecules are forced so close to each other that their arbitrary orientation is sterically hindered. Even at RT, the majority of the molecules is trapped in the potential minimum and forced into a long-range ordered phase. Now the Pauli repulsion regime of the potential becomes more and more dominant and finally the formation of two different high-coverage phases takes place, the relaxed and the

compressed monolayer structure, the latter defining the coverage of 1.00 ML. Their unit cell vectors are also located close to potential minima (not shown here).

We can conclude that the pair potential calculations explain the intermolecular interaction and the formation of the individual phases of CuPc/Au(111) very well. This is true for the repulsive interaction in the g-phase regime, the attractive interaction in the LT-phase, as well as the quantitative position of the phase boundary. The remarkable behavior of this system roots in the fact that the interplay of van der Waals and electrostatic interactions leads to a pair potential with specific attractive and repulsive regions, and the fact that the potential corrugations lie in the same range as the thermal energy kT.

V. CUPC/CU(111)

In Secs. III and IV, we demonstrated that our approach for pair potential calculations is well suited for model systems such as PTCDA/Au(111) and CuPc/Au(111), which represent physisorbed molecules on weakly interacting surfaces, although the lateral structure formation and the growth modes are fundamentally different for these two systems. One might expect that these kind of calculations are restricted to weakly interacting adsorbate systems, since any effect induced by the presence of the surface is neglected. On more strongly interacting surfaces such as Ag(111) or Cu(111), the structure formation is usually strongly influenced by the substrate. The exchange of charge between molecules and the substrate and the involved formation of interface dipoles is one of the key issues in this context. The interaction across the interface is usually site-specific, and hence, the structure of the substrate surface is often imposed onto the molecular layer leading to commensurate superlattices.

These effects can be seen for the adsorbate system CuPc/Cu(111). Both a partially occupied former lowest unoccupied molecular orbital (F-LUMO) occurring in the valence spectrum[10] and adsorption heights in the range of 2.5–2.8 Å found by XSW (Ref. 9) demonstrate the overlap of molecular wavefunctions with the substrate electronic states. This leads to a strong exchange of electronic charge, i.e., to chemisorption of the molecules. The structural phase diagram as well as the different phases themselves were subject of various investigations using SPA-LEED and UPS,[10] XSW,[9] as well as STM.[42] The formation of short molecular chains at (very) low coverages, and classical island formation in a commensurate structure at high coverages were observed. Both findings indicate an overall attractive intermolecular interaction for CuPc molecules on Cu(111), in contrast to the situation on Au(111) discussed above. This suggests that the attraction is induced by the strong chemisorptive interaction with the substrate.

We now try to understand this different behavior using a pair potential approach which takes substrate interaction into account by using a modified charge distribution in the molecular orbitals, based on the model of donation and back-donation of electronic charge.

The principle of donation/back-donation which describes the charge redistribution across the metal-organic interface was observed in recent experimental studies[7,8] for SnPc and CuPc on Ag(111), and in state-of-the-art quantum chemical calculations for PTCDA on noble metal surfaces.[43–45] The model is based on the overlap of all occupied molecular wavefunctions with the substrate causing donation of charge from the molecule into the substrate, and a back-donation of charge into the LUMO which, thus, becomes (partially) occupied. It could be demonstrated that donation and back-donation are of similar magnitude which leads to a rather small net charge transfer.[43–45] Furthermore, it is known that CuPc is a strong donor molecule, while UPS data show an almost fully occupied F-LUMO state.[10] Hence, for our calculations we assume a donation as well as a back-donation of $2e^-$ leading to a vanishing net charge transfer across the interface. We implemented this charge transfer by equally subtracting a partial charge of $2/n\ e^-$ from all n atoms which contribute to molecular orbitals significantly overlapping with the substrate. These are basically all atoms of the molecule (except the hydrogen atoms). A total charge of $2e^-$ is then added equally to all atoms contributing to the density of states of the LUMO.

From gas-phase DFT calculations,[27] it is known that the LUMO is a two-fold degenerate state as shown in Fig. 9(a). The sum of both LUMOs, therefore, has a four-fold symmetry (as the entire molecule). However, one key aspect for this system is that the four-fold symmetry is broken by the interaction of the molecule with a six-fold symmetric surface. This is also illustrated in Fig. 9(a). It can be seen that the registry of both LUMO states with the substrate atoms are different, which causes a different charge transfer from the surface states into both LUMO states. The consequence is that the symmetry of the adsorbed molecule is reduced to two-fold, which was demonstrated in an STM experiment by Karacuban *et al.*[42] The left part of Fig. 9(b) is a reproduction of their STM image clearly showing two-fold symmetric CuPc molecules adsorbed on a Cu(111) surface. Note that this is an empty-states STM image in which the unoccupied LUMO state appears bright. The corresponding occupied LUMO state is then located at the other molecular wings, oriented vertically in Fig. 9(b).

In our model, we consider this effect by only assuming back-donation of charge into *one* of the LUMO states. This leads to a two-fold symmetric charge distribution of the molecule and, thus, also to a two-fold symmetry of the calculated pair potential which is displayed in Fig. 9(c) for two equally oriented molecules. The corresponding LUMO, which was used for the back-donation of charge, is displayed in the inset.

The fundamental differences to the interaction potentials for CuPc/Au(111) (see Fig. 8) are obvious. Beside the different symmetry, there are large regions of repulsion (gray) and attraction (red), similar to the case of PTCDA shown in Fig. 4. The corrugation of the pair potential has six symmetrically inequivalent minima, three of them deeper than −30 meV, whereby the deepest is −53 meV. This indicates that clustering of molecules can also occur at RT. There is a limited number of possible geometric arrangements which allows us to predict the most likely geometry based on our pair potential calculations.

The STM image in Fig. 9(b) suggests that the CuPc molecules preferably align their molecular wings along the

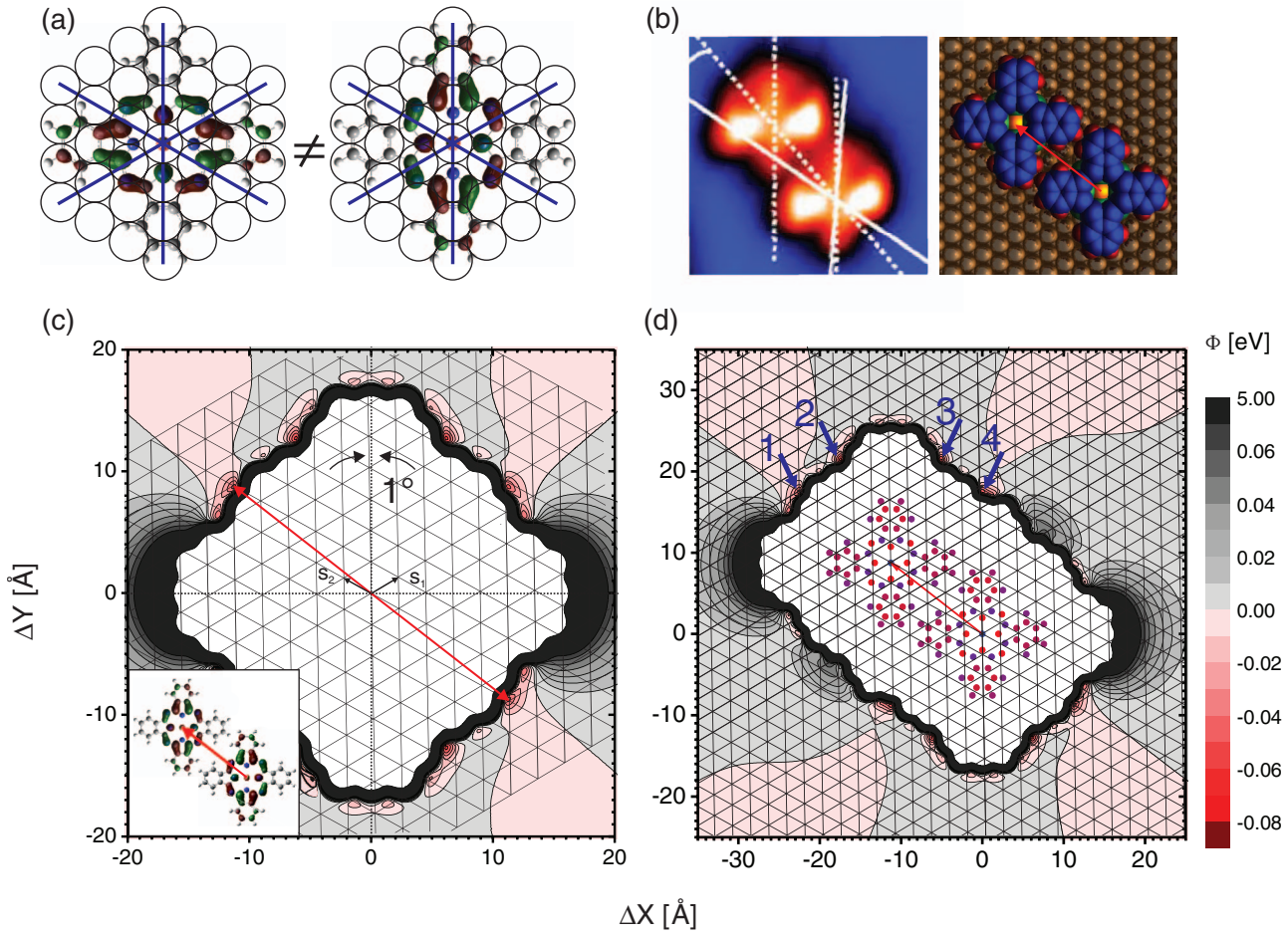

FIG. 9. (a) Illustration of the geometry of the two CuPc LUMO states which are degenerate in the gas phase. Their different registry with the substrate causes differences in the charge transfer with the surface and, therefore, lifts the degeneracy. (b) The favorable adsorption geometry (right) obtained from pair potential calculations agrees well with the experimental data. The empty-states STM image (left) is reproduced from Ref. 42. Dotted lines represent the molecular orientation, solid lines the direction of rows of copper atoms. (c) Pair potential map for the interaction of two equally oriented CuPc molecules including the modeled charge redistribution based on the donation/back-donation effect. (d) Pair potential map for the interaction between a third CuPc molecule that is attaching to a cluster of two molecules which are oriented according to the best configuration.

high symmetry direction of the substrate. This was observed with a precision of about 4°; this angle was found between the molecular symmetry axis and the substrate atomic rows in STM. Applying this observation to our calculations results in an orientation of the surface lattice as it is shown in Fig. 9(c) as a hexagonal net of thin black lines. It is remarkable that this orientation of the molecules brings one minimum of the potential map very close to a substrate lattice point. A twist of only 1° produces full coincidence of the lattice point with coordinates (1 6) in surface lattice units with the second-deepest minimum of the map, indicated by the red arrow. The consequence of such an arrangement is that all molecules have the same registry with the surface lattice (at higher coverages, one would call it a commensurate structure), which enables identical molecule-substrate interaction for all molecules and, hence, justifies the assumptions we made for our modeling regarding the charge transfer. Since this full coincidence is only found for one minimum, it suggests an identical relative position of neighboring molecules, i.e., an one-dimensional, chain-like arrangement as it is found experimentally for low coverages. A real space model showing this molecular arrangement is shown in the right of Fig. 9(b). It agrees very well with the corresponding STM image shown in the left.

We have investigated this trend to a chain-formation vs. island-like growth further. For this purpose, we have simulated the process of a third molecule attaching to a cluster of two molecules. In Fig. 9(d), the pair potential energy for such a scenario is shown: Two CuPc molecules are fixed at positions corresponding to their ideal situation (as shown in the center of the figure panel), the position of a third molecule relative to this cluster is varied. Again, a limited number of minima is found in this potential map, the deepest marked by small arrows and numbers in the figure. A comparison with Fig. 9(c) shows that the minima 1–3 are basically equivalent to the situation for two interacting molecules. Only minimum 4 is influenced, since in this position the third molecule interacts with both molecules significantly. Judging only the depth of the minima, one would expect the third molecule to attach at all of these minima, maybe preferably at no. 2 and 3. However, again taking the registry with the substrate into account,

there is only minimum 1 which allows molecule 3 to sit on a substrate lattice point and, hence, enables an identical registry of all three molecules with the surface lattice. Therefore, this minimum is preferred, which explains the chain formation observed experimentally.

Finally, we would like to mention that the same relative position of molecules can be found in the commensurate orthorhombic primitive ("op") and orthorhombic centered ("oc") phases observed for higher coverages by Stadtmüller *et al.*[10] This can easily be seen from the unit cell matrix of the op phase which is (6 2—1 6), i.e., it is spanned by the vectors (6 2) and (1 6). The latter has been identified as the ideal molecular distance vector from our pair potential calculations. Note that the shorter unit cell vector (6 2) lies in a region of Pauli repulsion close to a rather shallow minimum. It can be speculated that the molecules in this close-packed, compressed monolayer structure are slightly distorted which shifts the potential minimum close to this lattice point.

We can conclude that, based on the simplified charge redistribution model described above, the pair potential calculations can qualitatively explain the dominating intermolecular interaction of CuPc/Cu(111). They suggest a molecular arrangement of the molecules which is in good agreement with the basic experimental findings: Chain formation at low, commensurate islands at high coverages.

VI. SUMMARY

We have presented pair potential calculations based on van der Waals as well as electrostatic interaction between partial charges located at the individual atoms of the π-conjugated molecules PTCDA and CuPc. Using grid calculations, we obtain the ideal relative positions and orientations of the molecules which allows to draw conclusions on structure formation and growth mode in the submonolayer coverage regime.

For weakly interacting systems such as PTCDA/Au(111) and CuPc/Au(111), our calculations are in very good agreement with the experimental data. In the case of PTCDA/Au(111), the lateral structure as well as the stacking layer distance can be explained very well, whereby the interaction with up to six nearest neighbors is considered. For CuPc/Au(111), additionally the crossover from repulsive interaction (leading to a 2-dimensional gas-like phase) to attractive interaction (causing the condensation of the molecular film in well-ordered p.o.l. islands at LT) can be explained. Furthermore, even for a much more strongly interacting system such as CuPc/Cu(111), we can explain the relative molecular positions of the molecules in 1-dimensional chains at low coverage and in commensurate phases occurring above 0.76 ML. The interaction between molecules and surface, which cannot be neglected any more for this system, is estimated by a simplified model of charge donation from filled molecular orbitals into the surface on the one hand, and back-donation from the surface to the LUMO states on the other. Hereby, it was considered that the latter effect is not symmetric for both formerly degenerated LUMO states.

The results obtained for these selected examples demonstrate that our approach, in spite of its simplicity, represents a very promising tool for predicting structures of molecules physisorbed on weakly interacting surfaces, and – under some additional assumptions – also for chemisorbed molecules showing a charge transfer with the metal surface.

ACKNOWLEDGMENTS

We thank Christoph Kleimann for stimulating discussions. This work was supported by the Deutsche Forschungsgemeinschaft, project number KU 15312-1.

[1] F. S. Tautz, Prog. Surf. Sci. **82**, 479 (2007).
[2] N. Ueno and S. Kera, Prog. Surf. Sci. **83**, 490 (2008).
[3] G. Horowitz, R. Hajlaoui, R. Bourguiga, and M. Hajlaoui, Synth. Met. **101**, 401 (1999).
[4] J. Kido, M. Kimura, and K. Nagai, Science **267**, 1332 (1995).
[5] D. Dimitrakopoulos and P. Malenfant, Adv. Mater. **14**, 99 (2002).
[6] H. G. O. Sandberg, G. L. Frey, M. N. Shkunov, H. Sirringhaus, R. H. Friend, M. M. Nielsen, and C. Kumpf, Langmuir **18**, 10176 (2002).
[7] C. Stadler, S. Hansen, I. Kröger, C. Kumpf, and E. Umbach, Nat. Phys. **5**, 153 (2009).
[8] I. Kröger, B. Stadtmüller, C. Stadler, J. Ziroff, M. Kochler, A. Stahl, F. Pollinger, T. L. Lee, J. Zegenhagen, F. Reinert, and C. Kumpf, New J. Phys. **12**, 083038 (2010).
[9] I. Kröger, B. Stadtmüller, C. Kleimann, P. Rajput, and C. Kumpf, Phys. Rev. B **83**, 195414 (2011).
[10] B. Stadtmüller, I. Kröger, F. Reinert, and C. Kumpf, Phys. Rev. B **83**, 085416 (2011).
[11] K. Glöckler, C. Seidel, A. Soukopp, M. Sokolowski, E. Umbach, M. Böhringer, R. Berndt, and W. D. Schneider, Surf. Sci. **405**, 1 (1998).
[12] L. Kilian, E. Umbach, and M. Sokolowski, Surf. Sci. **600**, 2633 (2006).
[13] H. Marchetto, U. Groh, T. Schmidt, R. Fink, H. J. Freund, and E. Umbach, Chem. Phys. **325**, 178 (2006).
[14] M. Horn von Hoegen, Z. Kristallogr. **214**, 591 (1999).
[15] A. Hoshino, S. Isoda, H. Kurata, and T. Kobayashi, J. Appl. Phys. **76**, 4113 (1994).
[16] D. E. Hooks, T. Fritz, and M. D. Ward, Adv. Mater. **13**, 227 (2001).
[17] C. Stadler, S. Hansen, F. Pollinger, C. Kumpf, E. Umbach, T.-L. Lee, and J. Zegenhagen, Phys. Rev. B **74**, 035404 (2006).
[18] I. Kröger, P. Bayersdorfer, B. Stadtmüller, C. Kleimann, G. Mercurio, Y. Mi, P. Rajput, J. Zegehagen, F. Reinert, and C. Kumpf, Submonolayer growth of H_2-phthalocyanine on Ag(111), unpublished.
[19] I. Kröger, B. Stadtmüller, C. Stadler, C. Elsässer, and C. Kumpf, "Submonolayer and multilayer growth if TiO-phthalocyanine on Ag(111)" unpublished.
[20] C. Wagner, D. Kasemann, C. Golnik, R. Forker, M. Esslinger, K. Müllen, and T. Fritz, Phys. Rev. B **81**, 035423 (2010).
[21] R. S. Mulliken, J. Chem. Phys. **23**, 1833 (1955).
[22] J. P. Foster and F. Weinhold, J. Am. Chem. Soc. **102**, 7211 (1980).
[23] A. E. Reed and F. Weinhold, J. Chem. Phys. **78**, 4066 (1983).
[24] A. E. Reed, R. B. Weinstock, and F. Weinhold, J. Chem. Phys. **83**, 735 (1985).
[25] E. Martinez-Nunez, A. Rahaman, and W. L. Hase, J. Phys. Chem. C **111**, 354 (2007).
[26] S. Soubatch, I. Kröger, C. Kumpf, and F. S. Tautz, Phys. Rev. B **84**, 195440 (2011).
[27] J. Frisch, G. W. Trucks, H. B. Schlegel *et al.*, GAUSSIAN 03, Revision C.02, Gaussian, Inc., Wallingford, CT, 2004.
[28] C. Stadler, S. Hansen, A. Schöll, T.-L. Lee, J. Zegenhagen, C. Kumpf, and E. Umbach, New J. Phys. **9**, 50 (2007).
[29] J. Stanzel, W. Weigand, L. Kilian, H. L. Meyerheim, C. Kumpf, and E. Umbach, Surf. Sci. **571**, L311 (2004).
[30] R. A. Scott and H. A. Scheraga, J. Chem. Phys. **42**, 2209 (1965).
[31] J. C. Slater and J. G. Kirkwood, Phys. Rev. **37**, 682 (1931).
[32] A. K. Rappe, C. J. Casewit, K. S. Colwell, W. A. Goddard, and W. M. Skiff, J. Am. Chem. Soc. **114**, 10024 (1992).
[33] S. R. Forrest and Y. Zhang, Phys. Rev. B **49**, 11297 (1994).

[34]J. Shanker, P. S. Bakhshi, and L. P. Sharma, J. Inorg. Nucl. Chem. **41**, 1285 (1979).
[35]A. Bondi, J. Phys. Chem. **68**, 441 (1964).
[36]R. Temirov, S. Soubatch, O. Neucheva, A. C. Lassise, and F. S. Tautz, New J. Phys. **10**, 053012 (2008).
[37]C. Weiss, C. Wagner, C. Kleimann, M. Rohlfing, F. S. Tautz, and R. Temirov, Phys. Rev. Lett. **105**, 086103 (2010).
[38]C. Weiss, C. Wagner, R. Temirov, and F. S. Tautz, J. Am. Chem. Soc. **132**, 11864 (2010).
[39]G. Kichin, C. Weiss, C. Wagner, F. S. Tautz, and R. Temirov, J. Am. Chem. Soc. **133**, 16847 (2011).
[40]S. K. M. Henze, O. Bauer, T. L. Lee, M. Sokolowski, and F. S. Tautz, Surf. Sci. **601**, 1566 (2007).
[41]A. J. Lovinger, S. R. Forrest, M. L. Kaplan, P. H. Schmidt, and T. Venkatesan, J. Appl. Phys. **55**, 476 (1984).
[42]H. Karacuban, M. Lange, J. Schaffert, O. Weingart, Th. Wagner, and R. Möller, Surf. Sci. **603**, L393 (2009).
[43]A. Abbasi and R. Scholz, J. Phys. Chem. C **113**, 19897 (2009).
[44]L. Romaner, D. Nabok, P. Puschnig, E. Zojer, and C. Ambrosch-Draxl, New J. Phys. **11**, 053010 (2009).
[45]M. Rohlfing, R. Temirov, and F. S. Tautz, Phys. Rev. B **76**, 115421 (2007).
[46]It turned out that for finding the parameters from Eq. (3) for asymmetric pairs, the geometric rather than the arithmetic mean gives better results. In this case, the resulting potential minimum fits better the sum of empirical van der Waals radii.